AGU ADVANCING EARTH AND SPACE SCIENCE

Geophysical Research Letters®

RESEARCH LETTER
10.1029/2021GL094190

A Novel Method for Gaining New Insight on Flows Over Inundated Landscapes

Shailesh van der Steeg[1], Haiqing Xu[1,2], Raymond Torres[1], Edwin P. L. Elias[3], Jessica C. Sullivan[4], Enrica Viparelli[5], David Shelley[6], and Venkataraman Lakshmi[1,7]

[1]School of Earth, Ocean and Environment, University of South Carolina, Columbia, SC, USA, [2]School of Environment and Natural Resources, The Ohio State University, Columbus, OH, USA, [3]Deltares, Delft, The Netherlands, [4]Department of Biology & Geology, University of South Carolina Aiken, Aiken, SC, USA, [5]Department of Civil and Environmental Engineering, University of South Carolina, Columbia, SC, USA, [6]Old-Growth Bottomland Forest Research and Education Center, Hopkins, SC, USA, [7]Department of Engineering Systems and Environment, University of Virginia, Charlottesville, VA, USA

Key Points:

- Three depth sensors define an inundation free surface; the maximum gradient of the plane defines flow direction and magnitude
- Analysis of high-resolution flows helps fill a knowledge gap with temporal and spatial dynamics of floodplain inundation
- The controlling factors of floodplain flow dynamics are stage, rate of change of stage, and inundation process

Correspondence to:
S. van der Steeg,
svandersteeg@geol.sc.edu

Citation:
van der Steeg, S., Xu, H., Torres, R., Elias, E. P. L., Sullivan, J. C., Viparelli, E., et al. (2021). A novel method for gaining new insight on flows over inundated landscapes. *Geophysical Research Letters*, *48*, e2021GL094190. https://doi.org/10.1029/2021GL094190

Received 10 MAY 2021
Accepted 22 SEP 2021

Abstract We present a novel approach for detecting surface water flows over flooded terrain. The approach requires a minimum of three stage measurements and can be applied to any inundated surface, across a range of temporal and spatial scales. This method creates new and robust opportunities for field observation and for validation of numerical simulations and remote sensing analyses. In this proof-of-concept study, we found that floodplain free surface gradients were particularly variable during sub-bankfull inundation, including abrupt current reversals. Also, flow direction varied with stage and the rate of change in stage. The "triangular facet" approach provides a new type of mesoscale insight of flow processes over inundated landscapes, highlighting flow complexity. Moreover, the approach provides information on floods that represent a compromise between point velocimeter measurements and satellite remote sensing and it can provide substantial benefits to society by aiding in flood hazard and mitigation assessment and planning.

Plain Language Summary We present a new approach for estimating flow direction and speed over a flooded terrain using sets of three water level recorders arranged in a triangular configuration. The approach can be applied to any inundated surface and scaled as needed. The triangular facet method provides valuable field observations that can be used to assess the performance of numerical models or remote sensing data. In our application over an inundated floodplain, the approach revealed complex flow patterns in space and time, and it shows that flow configurations for a given water stage are not necessarily repeatable. In particular, during lower inundation depths, the flow directions were highly variable, including abrupt changes in flow direction. This work helps fill a knowledge gap with respect to circulation during floods that is critical to understanding hazard planning and mitigation, material cycling and floodplain processes, and functions and habitat sustainability.

1. Introduction

Low-relief and low-gradient landscapes, particularly along some continental margins, are increasingly susceptible to flooding, and this view is especially relevant given the role of modern climate change in compound flooding (IPCC, 2021). Floodplains are a distinct type of low-relief and low-gradient landscape with a land cover that can range from dense urban centers to largely uninhabited. Although floodplain floods may be considered natural hazards that affect many people at great cost, it has been shown that floodplains and floodplain processes provide substantial benefits to society (e.g., Jakubínský et al., 2021; Mazzoleni et al., 2021; Rak et al., 2016). Therefore, detailed insight on water circulation over inundated areas and the processes that facilitate inundation and drainage can aid in, for example, flood hazard and mitigation analyses and in maintaining floodplain ecosystems and water quality (e.g., Fischer et al., 2019; Funk et al., 2020; Osterkamp & Hupp, 2009). Moreover, despite their limited extent of ~0.5–1% of land area worldwide (e.g., Sutfin et al., 2016), they have a disproportionately large role in the global carbon cycle largely driven by cycles of inundation (e.g., D'Elia et al., 2017; Lininger et al., 2019; Sutfin et al., 2016).

Remote sensing of inundated floodplains reveals extensive temporal and spatial variability in water surface elevation and current direction (D. Alsdorf et al., 2007; D. E. Alsdorf et al., 2007; Mertes, 1997). The flow complexity is largely associated with spatially variable inundation that arises from a disequilibrium with the water surface of the main channel and the floodplain (D. E. Alsdorf et al., 2007). For instance, Filgueira-Rivera et al. (2007) show that elevations of the free surface between the main river and floodplain differ by up to 0.12 m, giving rise to complex flow patterns. Also, Girard et al. (2009) show that water surface elevation gradient across a river–floodplain system varied by a factor of ∼9. Further, numerical simulations of floodplain inundation suggest that the timing and pattern of flows are strongly influenced by the local, albeit low-relief geomorphic features (e.g., Czuba et al., 2019; Pinel et al., 2020).

Analyses of floodplain topography (David et al., 2017; Lindroth et al., 2020) and hydrodynamic modeling (Czuba et al., 2019) reveal that floodplain inundation occurs in the absence of overbank flow. These studies contrast with the typical view of inundation by overbank flows. In particular, sub-bankfull flows give rise to frequent, low-magnitude inundation (Czuba et al., 2019; Kaase & Kupfer, 2016; Park & Latrubesse, 2017). These observations are important because sub-bankfull flows facilitate a persistent hydraulic connectivity in floodplains (Passalacqua, 2017; Wohl et al., 2019) without overbank floods. Therefore, understanding floodplain inundation during low-frequency overbank inundation and high-frequency, but low-magnitude, sub-bankfull inundation is essential to understanding floodplain sustainability.

Although the above studies provide details on inundation pathways and dynamics, there remains a dearth of information on in situ flow paths at a scale suitable for the characterization of inundation and drainage processes. Therefore, advancements in understanding floodplain flow dynamics ultimately require detailed insight on floodplain inundation processes and pathways, and the hydraulic framework that drives them. Currently, gaining in situ knowledge on flow patterns and pathways requires the deployment of multiple velocimeters across the floodplain with the hope of measuring the dynamics of an anticipated flood event. However, despite the availability of fully autonomous current measuring devices, such as acoustic current profilers, the literature is completely devoid of such observations over floodplains. Part of the problem is likely related to the high cost of these devices (∼20 times the cost of sensors used here) and the researcher's limited ability to predict floodplain inundation events. Also, in deploying an autonomous device, the researcher must do an informal cost-benefit analysis that includes vandalism when the device is subaerial. This notwithstanding, acoustic devices have been used to show highly complex flow patterns for tidal inundations over salt marshes (e.g., Torres & Styles, 2007) and they reveal the important role of topography to inundation and drainage flow processes of an intertidal "floodplain." However, these approaches offer only point measurements and given the potential for acoustic interference by accumulations of large and small woody debris or sediment covering the acoustic sensor heads, the data may or may not be representative of actual floodplain flow conditions.

The work presented here introduces a low-cost, robust, in situ approach to estimating maximum free surface gradients that can help fill a knowledge gap on floodplain flow dynamics. Hence, this work is a proof-of-concept study for gaining mesoscale (∼0.01 km^2) insight on inundation that can help improve our understanding of flooding, circulation, and drainage processes over a complex, but low-relief and low-gradient floodplain. However, the approach can be applied to any inundated surface, at any field location and over a large range of spatial scales (e.g., >>0.01 km^2). We hypothesize that interactions of decimeter scale relief and water stage collectively impart complex flow patterns onto floodplain circulation, across a range of spatial and temporal scales. This hypothesis will be tested by analyzing maximum free surface gradient data from a range of inundation levels. In the following narrative, we use "gradient," "flow," and "vector" interchangeably for "the maximum free surface gradient" determined by the "triangular facet" approach.

2. Study Region and Hydrologic Conditions

The study site is a river-floodplain system of the southeastern North American coastal plain (Figure 1a), the Congaree River, SC, USA, in the Congaree National Park (CNP). The densely forested study site is 18.8 km long, and up to 5.9 km wide with a total area of 93 km^2. Mean floodplain valley elevation declines from 35.0 to 24.5 m giving an average valley gradient of 4×10^{-4} (Xu et al., 2020). The floodplain is bound by the Congaree River to the south and southwest and by bluffs to the north (Figure 1a).

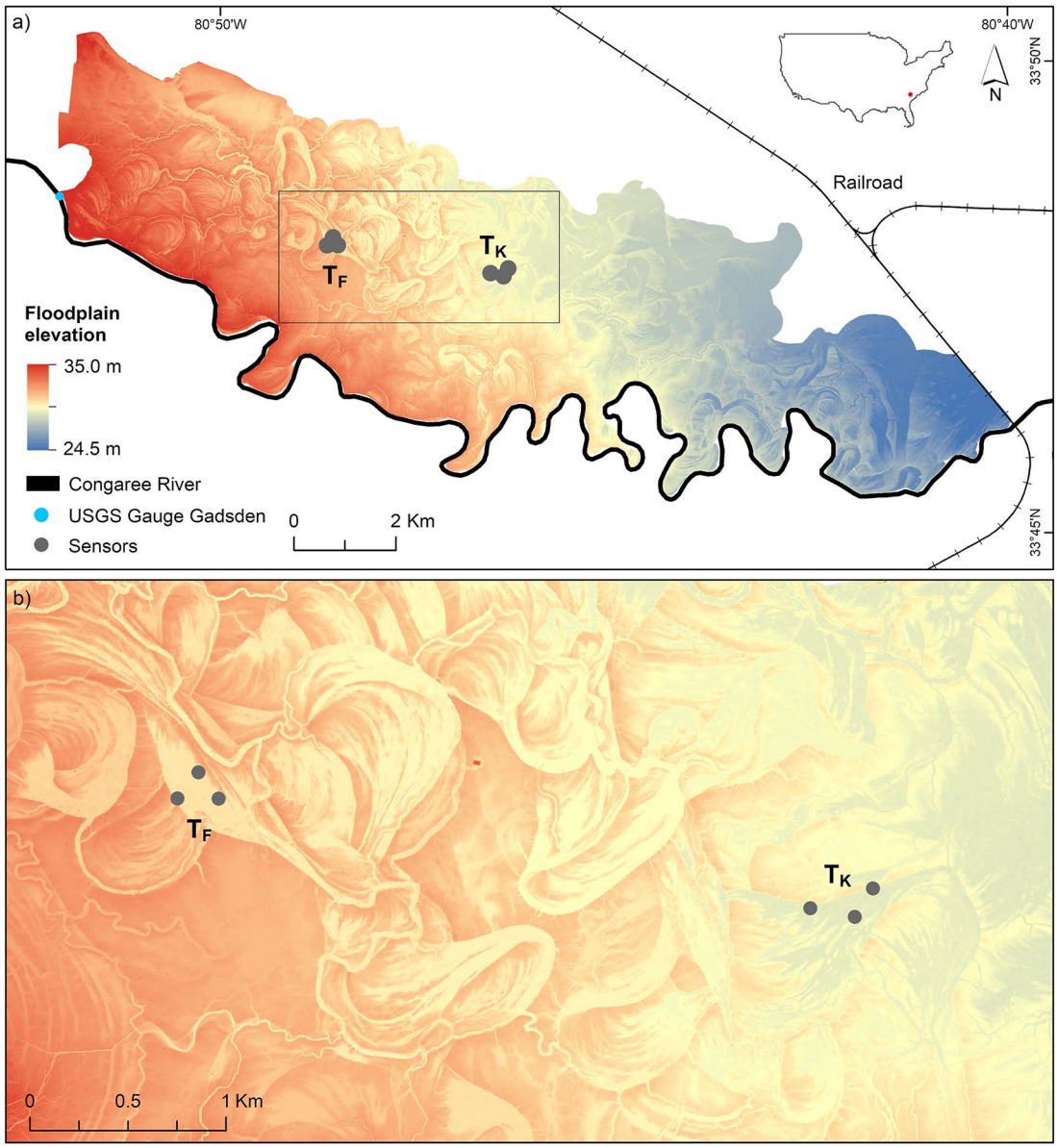

Figure 1. Study site. (a) Lidar DEM of the floodplain. Light green symbols show the location of water level sensors. Blue symbol is the United States Geological Survey (USGS) Gadsden station (#02169625). The inset map shows the location of Congaree National Park (CNP). (b) Subarea of the DEM showing the detailed topography around the sensors. The elevation within the subarea declines from 31.9 to 27.3 m.

The main channel along the CNP boundary is 39.1 km long with a gradient of 1.5×10^{-4}. Xu et al. (2020) showed that the bank elevation profile has a highly variable levee/bank crest height, thereby facilitating irregular along-channel inundation patterns. In particular, the levees in the upstream reach require a higher river stage for overbank inundation and therefore favor through-bank inundation, while in the downstream reach, the levees are lower and overbank inundation occurs at lower river stages (Xu et al., 2020). The locations for sub-bankfull inundation are the 32 well-developed through-bank channels, channels that cut through the local bank or levee, with mouth widths ranging from 7 to 30 m and some through-bank channels extend several kilometers into the floodplain interior. Hence, for a single discharge, floodplain inundation can occur by a combination of sub-bankfull and overbank flows (e.g., Lindroth et al., 2020).

The United States Geological Survey (USGS) Congaree River station in Columbia, SC (#02169500), provides the nearest long-term discharge record, 38 river kilometers upstream of the study site. Discharge from 1984 to 2020 range from 30 to 4,200 m^3/s with a median value of 146 m^3/s. Water levels at the USGS Gadsden

station (#02169625, Figure 1a) at the upstream park boundary show that the local stage (discharge not reported) varies by 8 m. We estimate that sub-bankfull inundations based on the Gadsden gauge occur 11% of the time, while overbank inundations occur at 5%.

3. Methodology

Water depths on the floodplain were measured using Onset HOBO U20 absolute pressure transducers (hereafter "sensors") set to record at 0.25-hr intervals. Sensors were deployed in protective enclosures, mounted to ∼1 m long stakes, and installed 2–3 km inland of the main channel, in subtle depressions (Figure 1a). Individual sensors have a typical accuracy of 0.004 m. The pressure readings were compensated for atmospheric pressure with an identical sensor deployed as a barometer. The resulting pressure readings were converted to water depth using the Onset HOBOware Pro software suite.

Each set of three sensors was arranged into a triangular configuration with the assumption that three sensor values define an average free surface plane; the triangle sites are French Pond (T_F) and Kingsnake (T_K; Figure 1a). The instrument accuracy has implications for the minimum detectable free surface gradient, and thus it influences the minimum distance between vertices of a triangle. Three sensors combined have a maximum error of 0.0069 m. To measure expected water surface slopes of $\sim 10^{-4}$ (e.g., the regional floodplain gradient) or larger, and accounting for propagation of uncertainty (Andraos, 1996) related to instrument accuracy and sensor deployment (e.g., GPS accuracy), we determined that the sensors must be placed a minimum of 123 m apart, giving an area of ∼0.0075 km^2 for an equilateral triangle. Error analyses show that these factors give rise to a maximum error of $\sim 10^{-8}$ for a free surface gradient of $\sim 10^{-4}$. The distances between sensors (Figure 1b), starting from the north, in an anticlockwise direction for T_F are 171, 210, and 170 m, respectively, with area and mean elevation of 0.018 km^2 and 27.82 m, respectively; meanwhile for T_K, the values are 330, 231, and 172 m and 0.014 km^2 and 28.79 m, respectively.

Computing free surface orientation requires that the corresponding depth data be referenced to a common vertical datum. After several field excursions, we determined that the forest canopy precludes the acquisition of high-precision GPS measurement of sensor elevation, even during winter, or "leaf-off" months. To circumvent this problem, we account for differences in elevation between sensors by referencing sensors of each triangle to a local static water surface. Here, we defined the steady-state stage for a "zero" elevation as an interval with maximum variations of 0.005 m over a period of 6 hr. We went on to determine the maximum free surface gradient magnitude and direction over specific inundation intervals. To enhance the visualization of graphical representations of results, vector thinning was applied to the 0.25-hr data; thus, we present one vector per 2-hr interval instead of eight (Figure 2).

This "triangular facet approach" is a novel application for defining inundation water free surface orientation, but it is identical to applications used to visualize groundwater flow dynamics (e.g., Freeze & Cherry, 1979) and coastal ocean gradients (Yankovsky, 2003). The main goal of our efforts is to capture the free surface gradients and maximum gradient direction every 0.25 hr as they vary with synchronous water level fluctuations at the vertices of the triangles. We assume that the inferred flow directions taken as the maximum gradient direction can be used to shed light on flow dynamics. Free surface gradients were only calculated when all sensors per triangle and corresponding areas were fully inundated.

Estimates of the free surface gradient allowed us to infer velocities computed with the Manning formula (e.g., Harvey et al., 2009). Note, however, that the computation of velocity is performed as a validation of the triangular facet approach to determine if the computed gradients give velocity values that are consistent with those in the literature. Application of the formula requires estimates of the hydraulic gradient and the Manning coefficient. We estimated the hydraulic radius as mean depth within a triangular array (e.g., US Department of Agriculture-Natural Resources Conservation Service, 2007). Roughness parameters are estimated based on the USGS (Arcement & Schneider, 1989) and we use $n = 0.11$ s/m$^{1/3}$, well within the range (0.015–0.40 s/m$^{1/3}$) reported in the literature (e.g., Czuba et al., 2019; Juez et al., 2019; Liu et al., 2019). Finally, rainfall-induced floodplain inundation is not considered here and its effects were excluded from all analyses of flow dynamics. The pluvial style of inundation generates a "bathtub-style" filling of the basin (e.g., Williams & Lück-Vogel, 2020) as opposed to a wave advancing over the floodplain (e.g., González-Sanchis et al., 2012), the latter being the main focus of this work.

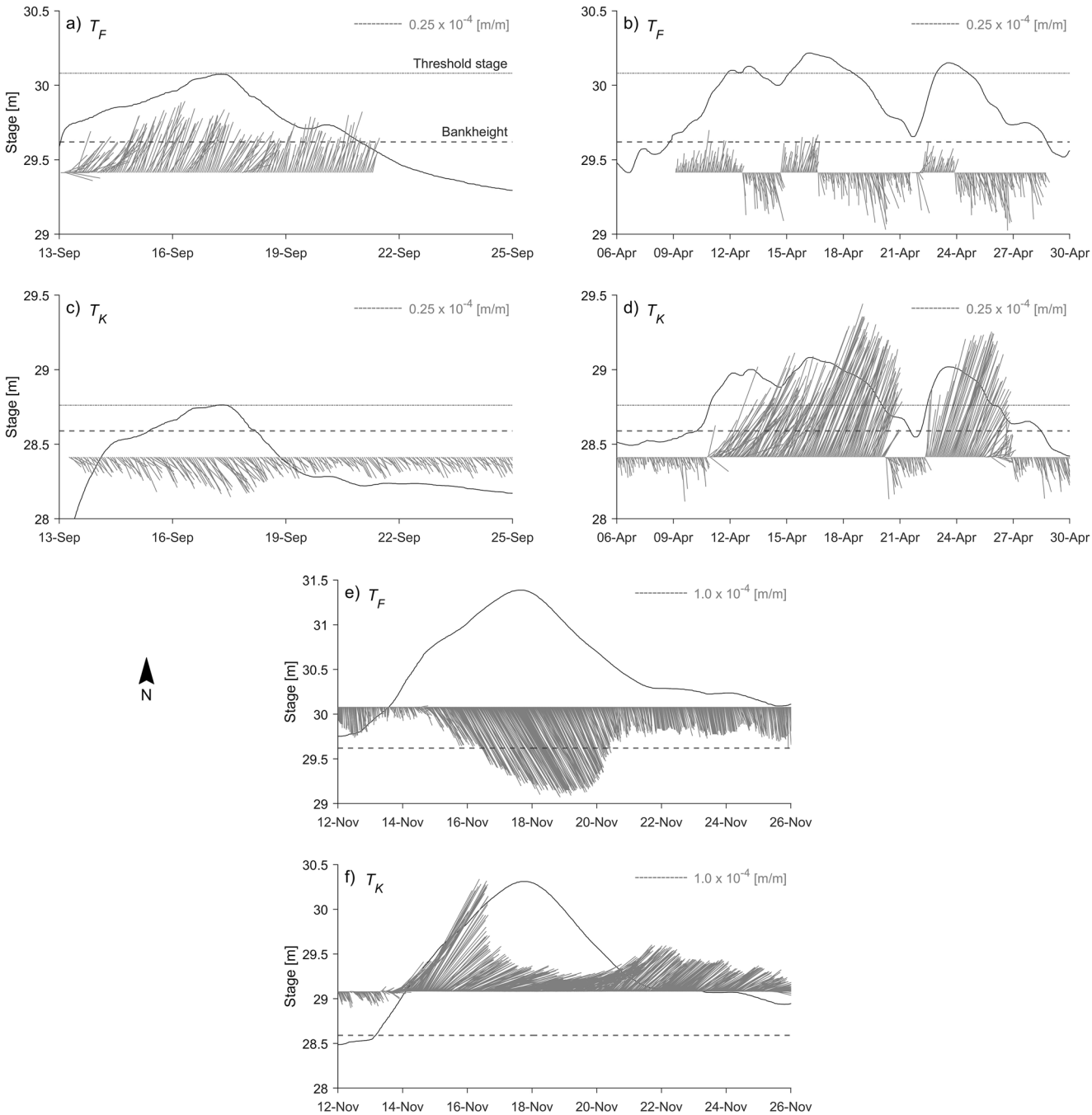

Figure 2. Flow dynamics of sub-bankfull inundation at T_F (a, b for different stages), sub-bankfull inundation at T_K (c, d for different stages), and overbank inundation at T_F (e) and T_K (f). The black line indicates the maximum stage hydrograph observed within a triangular facet. The horizontal dashed lines indicate average depression height containing the triangular arrays. The horizontal dashed-dotted line indicates a threshold stage. Gray vectors indicate magnitude and direction, with north at the top. Note that due to thinning of the data, each vector represents a 2-hr interval.

Analyses of free surface gradients, flow directions, and velocity estimates were performed for sub-bankfull and overbank flow conditions. River water depth measurements and bank elevations at six locations along the main channel were collected and converted to a common vertical reference using a high-precision GPS (horizontal and vertical accuracy ±0.015 and 0.025 m, respectively). Bank elevations and water level readings were combined to determine the occurrence of sub-bankfull or overbank flow conditions. Sub-bankfull flow conditions occur when water levels at the Gadsden gauge are between 29.95 and 31.54 m, while

overbank flow occurs when water levels exceed 31.54 m. Field observations indicate that the area around the sensors is fully submerged at stages that exceed ~1.0 m (Figure 1b).

4. Results

Free surface gradients range from 0.1 to 2.27 × 10^{-4}, and the inferred flow directions reveal several levels of complexity, from subtle reorientations with stage to complete current reversals. We elaborate on these findings by evaluating the stage hydrographs in response to two sub-bankfull inundation intervals for local water depths reaching 1.0–1.1 m (Figures 2a–2d). In both cases, stage increases at approximately the same rate from September 14 to 17 before reaching a single peak of ~1.0 m. Thereafter, a concave-up recession occurs, although a break in slope on September 20 is not apparent in both (Figures 2a–2d). The April 6–30 hydrographs are similar showing the stage increasing from about 0.5 to 1.1 m, and with three peaks several days apart (Figures 2b and 2d), followed by a much steeper recession rate.

4.1. Sub-Bankfull Inundation

For T_F stages <29.58 m, one sensor is subaerial and the data are not analyzed (Figure 2a). Above 29.58 m, the sub-bankfull inundation flow paths are initially eastward but become directed northward, with a slight component in the down valley direction (Figure 2a). Within this general trend are approximately day-long intervals where the free surface gradients develop a greater downslope component or 20°–30° rotation eastward. The gradient magnitude generally increases with stage. It has a mean of 0.23 × 10^{-4} ± 0.084 × 10^{-4} and a maximum of 0.49 × 10^{-4}. Note that maximum gradients precede maximum stage by about 1 day (Figure 2a). Flow paths directed northward occur once the stage exceeds ~29.62 m, the elevation of the northern edge of the local depression (Figure 1b). On the other hand, at a slightly higher sub-bankfull stage, the time series of T_F flow vectors (Figure 2b) differ substantially from the lower hydrograph stage. At stages >30.08 m, flow directions shift between northerly and southerly trends, and each cycle persists for >1.5 days (Figure 2b). In particular, during the rising stages of the three peaks, the flows are to the north, while during recession they are to the south (Figure 2b). Gradients associated with the falling limbs are slightly larger than during the rising limb, with a mean of 0.11 × 10^{-4} ± 0.069 × 10^{-4} and a maximum of 0.43 × 10^{-4}.

At T_K, for stages of about 27.98–28.76 m, flow directions are largely to the southeast, with occasional rotations to the east-southeast (Figure 2c). The gradient values vary within a range of 1.1 × 10^{-4} and seem independent of stage and rate of change in stage. However, as the stage approaches 28.76 m, the vectors become proportional to stage height, but peak stage occurs about one half-day after peak gradient. On the other hand, for the slightly higher hydrograph of April, flows differ substantially for stage >28.76 m (Figure 2d). From April 6 to 11, weak flows are to the south, but on ~April 11, there is a short-lived factor of 3 increase in southerly gradient that precedes a current reversal (Figure 2d). From April 11 to 20, flows are to the northeast and gradients appear strongly correlated with stage, and the cycle is repeated. Flow paths are directed northeast when stage exceeds bank elevation (Figure 1b). This is in stark contrast to flow paths for stages <28.76 m (Figure 2c), where flow paths continue southeast, even after the stage exceeds the local bank elevation. Mean and maximum gradients during lower stages are 0.1 × 10^{-4} ± 0.061 × 10^{-4} and a maximum of 0.36 × 10^{-4}, which are substantially smaller than observed during higher, albeit sub-bankfull flow, where gradients have a mean 0.39 × 10^{-4} ± 0.32 × 10^{-4} and maximum 1.1 × 10^{-4}.

In summary, the sub-bankfull inundation process gives rise to temporally and spatially complex flow patterns identified through analyses of free surface gradients. The flow system complexity is exemplified through current reversals that occur in response to a threshold in stage. On the other hand, at lower levels of inundation, flows tend to have a preferred orientation, mostly to the south. Also, hydrograph peaks have a maximum gradient that is not correlated with maximum stage; in one example, it precedes the maximum and in the other it occurs after the peak has passed.

4.2. Overbank Inundation

Overbank flows are apparent as a ~2 m rise in stage at both T_F and T_K (Figures 2e and 2f), and gradient magnitudes have a mean of $0.80 \times 10^{-4} \pm 0.62 \times 10^{-4}$ and a maximum of 2.18×10^{-4}. During November 12–15, the gradients are initially low, but they double within a day before declining to below the initial values by November 14.5. Thereafter, they steadily increase and attain peak values that correspond with the peaks in the hydrographs at ~31.39 m on November 18. The gradual increase is accompanied by a ~20° easterly rotation before returning to due south on November 21 when the stage is at 30.20 m. Overall, for site T_F, the response is substantially subdued relative to the sub-bankfull responses (Figures 2a and 2b).

As with T_F, the gradients for T_K are initially small, the lowest gradients directed southward (Figure 2f). After 2 days, the vectors rotate >90° resulting in north-northeasterly flows, and they increase with stage, reaching a maximum value at less than halfway along the rising limb. As stage continues to rise, flows rotate to the east and gradients decline; hence, the peak gradient precedes peak stage by nearly 4 days. As the stage continues to rise, the flows become more easterly until November 20 when the falling limb stage is at ~29.49 m. Thereafter, the gradients are to the northeast with a declining stage (Figure 2f). Overall, gradients are not directly associated with stage, with a maximum of 2.72×10^{-4} and gradients do not acquire similar magnitudes during the falling as for the rising limb, for the same stage. The mean gradient is $1.31 \times 10^{-4} \pm 0.57 \times 10^{-4}$. The occurrence of the magnitude maximum during early increase in stage is different from observed gradients during sub-bankfull inundation and for T_F (Figure 2e), where gradients appear to be proportional to stage.

In summary, inundation by overbank flow leads to inconsistent maximum gradient responses between sites. In one case, maximum gradient is directly proportional to stage, while in the other the relationship is the inverse. Moreover, despite the higher overbank stage, the maximum gradients are associated with sub-bankfull flow. On the other hand, flow reversals are limited to sub-bankfull conditions, although there is substantial flow vector reorientation for bankfull.

4.3. Flow Velocity

At site T_F, for stages <30.08 m, maximum flow velocity of 0.06 m/s occurs at a stage of 30.03 m on the rising limb, and it is northward, while average velocity is 0.03 ± 0.01 m/s (Figure 2a). For depths >30.08 m, but still sub-bankfull, the largest velocities occur at a stage of 30.21 m, reaching 0.06 m/s, while the mean velocity is 0.02 ± 0.01 m/s (Figure 2b). For overbank inundation, a velocity maximum of 0.23 m/s occurs, while it averages 0.10 ± 0.06 m/s, and the largest velocity is obtained at a stage of 31.13 m prior to the maximum stage (Figure 2e).

For site T_K, at <28.76 m stage, flow is limited to 0.04 m/s with a mean of 0.01 ± 0.001 m/s. Maximum velocity of 0.04 m/s occurs at a stage of 28.61 m, during falling stages and is toward the southeast (Figure 2c). For the slightly higher hydrograph, depths >28.76 m result in a maximum velocity of 0.11 m/s with an average of 0.05 ± 0.03 m/s (Figure 2d); maximum velocity precedes maximum stage. Overbank inundation results in an average velocity of 0.13 ± 0.06 m/s with a maximum of 0.22 m/s. The magnitudes of velocity appear to be related to stage, with the maximum velocity occurring at maximum depth, likely resulting from the effects of increased depth in the Manning expression. Overall, these estimated velocities compare favorably with those reported from floodplain field studies giving a range of 0.01–0.67 m/s (Arcement & Schneider, 1989; Girard et al., 2009; Harvey et al., 2009).

Overall, we apply a technique novel to floodplain research to show that floodplain flows can be predictably simple and highly complex in time and space. We found that the controlling factors on flow dynamics are largely a function of stage and rate of change of stage, where the rate of change is largely controlled by the style of inundation. In particular, we show that sub-bankfull inundation and overbank inundation influence the rate and magnitude of changes in stage and these, in turn, impart distinctly different features to the prevailing flows (Figures 2a–2d vs. Figures 2e and 2f).

5. Discussion and Interpretations

To glean deeper insight into processes governing the wetting, circulation, and draining of inundated landscapes, we present a method that is a compromise in spatial scale between point measurements from acoustic devices and satellite remote sensing of water surfaces, the two most common approaches of direct measurement. Given the minimum surface area of individual sensor deployment triangles, we propose that the triangular facet provides "mesoscale" observations of average flow conditions. Moreover, in assessing system flow dynamics, these free surface measurements can be considered, at times, superior to point measurements from velocimeters as acoustic signals can be degraded by large and small floating debris or sediment accumulation on acoustic sensor heads. In these cases, the pressure sensors are only marginally affected. Also, the facet data provide a tremendous advance over satellite remote sensing in that the latter may be complicated by forest canopy or are acquired over a large spatial scale. Finally, the facet data can be acquired every few minutes, much more frequently than satellite passes. Overall, the facet approach creates new research opportunities for inundated landscape hydrodynamics. Also, the facet approach has inherent flexibility in that any number of pressure sensors can be arranged in any number of configurations, and within each configuration occurs multiple sets of adjacent triangles. Hence, the facet approach can promote the creation of new knowledge on local to broader scale flow dynamics over inundated landscapes.

Although the facet method does not provide direct point measurements of water velocity, or velocity profiles, as with autonomous acoustic devices, it could be used to augment such measurements over larger spatial scales. Additionally, acoustic devices that record velocity data at the 0.25-hr interval of this study will have a limited battery life of ∼0.1 year, whereas the pressure transducers used here can record data for ∼1.5 years before running out of memory. This notwithstanding, we propose that a combination of acoustic and facet field data can be expected to more fully represent complex flow systems or system dynamics, and thereby shed greater light on, for example, floodplain hydraulic connectivity, a topic of increased interest requiring transdisciplinary approaches over small and large temporal and spatial scales (e.g., Passalacqua et al., 2017; Wohl et al., 2019).

At our floodplain study site, the gradients computed at T_F and T_K for sub-bankfull flows show that local flow dynamics are threshold dependent. The threshold is governed by the elevation at which flows in floodplain networks merge and inundate the local topography, similar to the initiation of infiltration excess overland flow that occurs with the infilling of local storage (e.g., Horton overland flow). Further, field observations reveal that channel networks at each site become connected at different stages and flow during low stages the connections occur through channel networks. When the stage exceeds the threshold, the free surface gradients of the rising limb may be nearly opposite or perpendicular to directions observed on the falling limb. Meanwhile with stage below the threshold values, the flow orientations are approximately uniform (Figure 2). Therefore, we infer that the channel network-linking determines and limits potential flow pathways, and thus control directional variability.

Moreover, we demonstrate the utility of the triangular facet approach to estimating flow direction and speed that are representative of mesoscale flows averaged over ∼0.01 km^2. This approach and corresponding results are not limited by the uncertainties of decimeter or small-scale point measurements of acoustic devices, nor the impediments to acquiring remote sensing data. The facet approach provides new knowledge with respect flow dynamics. Further, this mesoscale insight provides a foundation for an improved understanding of floodplain dynamics and hydraulic connectivity of a floodplain (e.g., Wohl, 2017) at a much higher temporal frequency than can be acquired with satellite remote sensing, and at a much finer spatial resolution.

Overall, we show that flows and currents estimated with the facet approach shed light on understanding flow processes, and can be used to help guide the development of hydrodynamic models, and help target questions to be addressed through simulations. For example, the approach can identify locations where a highly resolved computational domain of subtle topographic features may be necessary to detect and understand the role of complex mesoscale hydrodynamic processes in floodplain hydraulic connectivity, ecosystem responses, and floodplain sustainability. Further, the corresponding stage, gradient, and flow direction data provide a robust data set necessary to effectively assess a model's capability of resolving spatial variation floodplain hydrodynamics. We contend that the combination of multiple pressure readings and

corresponding flow directions and inferred velocities that all arise from the application of the facet method can enhance validation of numerical simulations and thereby improve their representation of actual field conditions (e.g., Czuba et al., 2019; Kupfer et al., 2015). Hence, the "triangular facet" approach to assessing inundated landscape flow dynamics helps fill a knowledge gap regarding inundation–drainage processes and it provides multiple data sets for model and remote sensing validations.

6. Conclusions

An in situ three-point approach for the estimation of mesoscale (~0.01 km^2) free surface gradients and flow directions for inundated landscapes is presented as the "triangular facet approach." Analyses of the maximum gradient data acquired at, and averaged over, 0.25-hr intervals show that floodplain flows can be predictably simple or complex, for different water stages and between locations, and the effects are largely controlled by inundation process. Flows during sub-bankfull inundation are particularly variable, including multiple abrupt flow reversals, while overbank inundation gives a more subdued response with slow ~90° rotations. During sub-bankfull inundation, the local relic geomorphic structures influence flows that are routed through the floodplain interior. However, with higher overbank flows, the rate of change of stage is a more important driver of flow complexity than local relief. Overall, the triangular facet approach provides robust information on flow dynamics that can greatly enhance the utility of data from satellite remote sensing and acoustic current measuring devices, and numerical simulations of flow.

Data Availability Statement

The lidar data set are available from NOAA Digital Coast website at https://chs.coast.noaa.gov/htdata/lidar1_z/geoid18/data/4815/. The river stage and discharge records at the USGS stations are available at https://waterdata.usgs.gov/sc/nwis/uv?site_no=02169625 (Congaree River at Columbia, SC) and at https://nwis.waterdata.usgs.gov/nwis/inventory/?site_no=02169625 (Congaree River at Congaree National Park near Gadsden, SC). All water depth data are available at https://doi.org/10.4211/hs.eab35a0af8104dd5921ef3ebbefddd87. All URLs were accessible as of August 15, 2021.

Acknowledgments
This work was initiated with NSF RAPID award 1604063 and later supported by NASA SC EPSCoR award NNX-16AR02A and NSF CBET 1751926.

References

Alsdorf, D., Bates, P., Melack, J., Wilson, M., & Dunne, T. (2007). Spatial and temporal complexity of the Amazon flood measured from space. *Geophysical Research Letters*, *34*, L08402. https://doi.org/10.1029/2007GL029447

Alsdorf, D. E., Rodríguez, E., & Lettenmaier, D. P. (2007). Measuring surface water from space. *Reviews of Geophysics*, *45*, RG2002. https://doi.org/10.1029/2006RG000197

Andraos, J. (1996). On the propagation of statistical errors for a function of several variables. *Journal of Chemical Education*, *73*(2), 150. https://doi.org/10.1021/ed073p150

Arcement, G. J., & Schneider, V. R. (1989). *Guide for selecting Manning's roughness coefficients for natural channels and flood plains*.

Czuba, J. A., David, S. R., Edmonds, D. A., & Ward, A. S. (2019). Dynamics of surface-water connectivity in a low-gradient meandering river floodplain. *Water Resources Research*, *55*, 1849–1870. https://doi.org/10.1029/2018WR023527

David, S. R., Edmonds, D. A., & Letsinger, S. L. (2017). Controls on the occurrence and prevalence of floodplain channels in meandering rivers. *Earth Surface Processes and Landforms*, *42*(3), 460–472. https://doi.org/10.1002/esp.4002

D'Elia, A. H., Liles, G. C., Viers, J. H., & Smart, D. R. (2017). Deep carbon storage potential of buried floodplain soils. *Scientific Reports*, *7*(1), 1–7.

Filgueira-Rivera, M., Smith, N. D., & Slingerland, R. L. (2007). Controls on natural levee development in the Columbia River, British Columbia, Canada. *Sedimentology*, *54*(4), 905–919. https://doi.org/10.1111/j.1365-3091.2007.00865.x

Fischer, C., Damm, C., Foeckler, F., Gelhaus, M., Gerstner, L., Harris, R., et al. (2019). The "habitat provision" index for assessing floodplain biodiversity and restoration potential as an ecosystem service—Method and application. *Frontiers in Ecology and Evolution*, *7*, 483. https://doi.org/10.3389/fevo.2019.00483

Freeze, A., & Cherry, J. (1979). *Groundwater*. Prentice-Hall.

Funk, A., Tschikof, M., Grüner, B., Böck, K., Hein, T., & Bondar-Kunze, E. (2020). Analysing the potential to restore the multi-functionality of floodplain systems by considering ecosystem service quality, quantity and trade-offs. *River Research and Applications*, *37*(2), 221–232. https://doi.org/10.1002/rra.3662

Girard, P., Fantin-Cruz, I., De Oliveira, S. M. L., & Hamilton, S. K. (2009). Small-scale spatial variation of inundation dynamics in a floodplain of the Pantanal (Brazil). *Hydrobiologia*, *638*(1), 223–233. https://doi.org/10.1007/s10750-009-0046-9

González-Sanchis, M., Murillo, J., Latorre, B., Comín, F., & García-Navarro, P. (2012). Transient two-dimensional simulation of real flood events in a Mediterranean floodplain. *Journal of Hydraulic Engineering*, *138*(7), 629–641. https://doi.org/10.1061/(ASCE)HY.1943-7900.0000565

Harvey, J. W., Schaffranek, R. W., Noe, G. B., Larsen, L. G., Nowacki, D. J., & O'Connor, B. L. (2009). Hydroecological factors governing surface water flow on a low-gradient floodplain. *Water Resources Research*, *45*, W03421. https://doi.org/10.1029/2008WR007129

IPCC. (2021). *Climate change 2021: The physical science basis. Contribution of Working Group I to the Sixth Assessment Report of the Intergovernmental Panel on Climate Change*. Cambridge University Press.

Jakubínský, J., Prokopová, M., Raška, P., Salvati, L., Bezak, N., Cudlín, O., et al. (2021). Managing floodplains using nature-based solutions to support multiple ecosystem functions and services. *Wiley Interdisciplinary Reviews: Water*, *8*(5), e1545. https://doi.org/10.1002/wat2.1545

Juez, C., Schärer, C., Jenny, H., Schleiss, A. J., & Franca, M. J. (2019). Floodplain land cover and flow hydrodynamic control of overbank sedimentation in compound channel flows. *Water Resources Research*, *55*, 9072–9091. https://doi.org/10.1029/2019WR024989

Kaase, C. T., & Kupfer, J. A. (2016). Sedimentation patterns across a Coastal Plain floodplain: The importance of hydrogeomorphic influences and cross-floodplain connectivity. *Geomorphology*, *269*, 43–55. https://doi.org/10.1016/j.geomorph.2016.06.020

Kupfer, J. A., Meitzen, K. M., & Gao, P. (2015). Flooding and surface connectivity of *Taxodium-Nyssa* stands in a southern floodplain forest ecosystem. *River Research and Applications*, *31*(10), 1299–1310. https://doi.org/10.1002/rra.2828

Lindroth, E. M., Rhoads, B. L., Castillo, C. R., Czuba, J. A., Güneralp, İ., & Edmonds, D. (2020). Spatial variability in bankfull stage and bank elevations of lowland meandering rivers: Relation to rating curves and channel planform characteristics. *Water Resources Research*, *56*, e2020WR027477. https://doi.org/10.1029/2020WR027477

Lininger, K. B., Wohl, E., Rose, J. R., & Leisz, S. J. (2019). Significant floodplain soil organic carbon storage along a large high-latitude river and its tributaries. *Geophysical Research Letters*, *46*, 2121–2129. https://doi.org/10.1029/2018GL080996

Liu, Z., Merwade, V., & Jafarzadegan, K. (2019). Investigating the role of model structure and surface roughness in generating flood inundation extents using one- and two-dimensional hydraulic models. *Journal of Flood Risk Management*, *12*(1), e12347. https://doi.org/10.1111/jfr3.12347

Mazzoleni, M., Mård, J., Rusca, M., Odongo, V., Lindersson, S., & Di Baldassarre, G. (2021). Floodplains in the Anthropocene: A global analysis of the interplay between human population, built environment, and flood severity. *Water Resources Research*, *57*, e2020WR027744. https://doi.org/10.1029/2020WR027744

Mertes, L. A. (1997). Documentation and significance of the perirheic zone on inundated floodplains. *Water Resources Research*, *33*(7), 1749–1762. https://doi.org/10.1029/97WR00658

Osterkamp, W. R., & Hupp, C. R. (2009). Fluvial processes and vegetation—Glimpses of the past, the present, and perhaps the future. *Geomorphology*, *116*(3–4), 274–285. https://doi.org/10.1016/j.geomorph.2009.11.018

Park, E., & Latrubesse, E. M. (2017). The hydro-geomorphologic complexity of the lower Amazon River floodplain and hydrological connectivity assessed by remote sensing and field control. *Remote Sensing of Environment*, *198*, 321–332. https://doi.org/10.1016/j.rse.2017.06.021

Passalacqua, P. (2017). The Delta Connectome: A network-based framework for studying connectivity in river deltas. *Geomorphology*, *277*, 50–62. https://doi.org/10.1016/j.geomorph.2016.04.001

Pinel, S., Bonnet, M. P., Da Silva, S. J., Sampaio, T. C., Garnier, J., Catry, T., et al. (2020). Flooding dynamics within an Amazonian floodplain: Water circulation patterns and inundation duration. *Water Resources Research*, *56*, e2019WR026081. https://doi.org/10.1029/2019WR026081

Rak, G., Kozelj, D., Steinman, F., Sutfin, N. A., Wohl, E. E., & Dwire, K. A. (2016). The impact of floodplain land use on flood wave propagation. *Natural Hazards*, *83*(1), 425–443. https://doi.org/10.1007/s11069-016-2322-0

Sutfin, N. A., Wohl, E. E., & Dwire, K. A. (2016). Banking carbon: A review of organic carbon storage and physical factors influencing retention in floodplains and riparian ecosystems. *Earth Surface Processes and Landforms*, *41*(1), 38–60. https://doi.org/10.1002/esp.3857

Torres, R., & Styles, R. (2007). Effects of topographic structure on salt marsh currents. *Journal of Geophysical Research*, *112*, F02023. https://doi.org/10.1029/2006JF000508

US Department of Agriculture-Natural Resources Conservation Service (USDA-NRCS). (2007). Stream restoration design. In *Part 654 of the National engineering handbook (210-VI-NEH)*.

Williams, L. L., & Lück-Vogel, M. (2020). Comparative assessment of the GIS based bathtub model and an enhanced bathtub model for coastal inundation. *Journal of Coastal Conservation*, *24*(2), 1–15. https://doi.org/10.1007/s11852-020-00735-x

Wohl, E. (2017). Connectivity in rivers. *Progress in Physical Geography*, *41*(3), 345–362. https://doi.org/10.1177/0309133317714972

Wohl, E., Brierley, G., Cadol, D., Coulthard, T. J., Covino, T., Fryirs, K. A., et al. (2019). Connectivity as an emergent property of geomorphic systems. *Earth Surface Processes and Landforms*, *44*, 4–26. https://doi.org/10.1002/esp.4434

Xu, H., van der Steeg, S., Sullivan, J., Shelley, D., Cely, J. E., Viparelli, E., et al. (2020). Intermittent channel systems of a low-relief, low-gradient floodplain: Comparison of automatic extraction methods. *Water Resources Research*, *56*, e2020WR027603. https://doi.org/10.1029/2020WR027603

Yankovsky, A. E. (2003). The cold-water pathway during an upwelling event on the New Jersey shelf. *Journal of Physical Oceanography*, *33*(9), 1954–1966. https://doi.org/10.1175/1520-0485(2003)033<1954:TCPDAU>2.0.CO;2